



Published in final edited form as:

*Magn Reson Med.* 2014 February ; 71(2): 815–822. doi:10.1002/mrm.24683.

## Accelerated Isotropic Sub-Millimeter Whole-Heart Coronary MRI: Compressed Sensing versus Parallel Imaging

Mehmet Akçakaya<sup>1</sup>, Tamer A. Basha<sup>1</sup>, Raymond H. Chan<sup>1</sup>, Warren J. Manning<sup>1,2</sup>, and Reza Nezafat<sup>1</sup>

<sup>1</sup>Department of Medicine (Cardiovascular Division), Beth Israel Deaconess Medical Center and Harvard Medical School, Boston, MA

<sup>2</sup>Department of Radiology, Beth Israel Deaconess Medical Center and Harvard Medical School, Boston, MA

### Abstract

**Purpose**—To enable accelerated isotropic sub-millimeter whole-heart coronary MRI within a six-minute acquisition, and to compare this with a current state-of-the-art accelerated imaging technique at acceleration rates beyond what is used clinically.

**Methods**—Coronary MRI still faces major challenges, including lengthy acquisition time, low signal-to-noise-ratio (SNR), and suboptimal spatial resolution. Higher spatial resolution in the sub-millimeter (sub-mm) range is desirable, but this results in increased acquisition time and lower SNR, hindering its clinical implementation. In this study, we sought to utilize an advanced  $B_1$ -weighted compressed sensing (CS) technique for highly-accelerated sub-mm whole-heart coronary MRI, and to compare the results to parallel imaging, the current-state-of-the-art, where both techniques were used at acceleration rates beyond what is used clinically. Two whole-heart coronary MRI datasets were acquired in seven healthy adult subjects ( $30.3 \pm 12.1$  yrs; 3 men), using prospective 6-fold acceleration, with random undersampling for the proposed CS technique and with uniform undersampling for SENSE reconstruction. Reconstructed images were qualitatively compared in terms of image scores and perceived SNR on a 4-point scale (1 = poor, 4 = excellent) by an experienced blinded reader.

**Results**—The proposed technique resulted in images with clear visualization of all coronary branches. Overall image quality and perceived SNR of the CS images were significantly higher than those of parallel imaging ( $P=0.03$  for both), which suffered from noise amplification artifacts due to the reduced SNR.

**Conclusion**—The proposed CS-based reconstruction and acquisition technique for sub-mm WH coronary MRI provides 6-fold acceleration, where it outperforms parallel imaging with uniform undersampling.

## Keywords

compressed sensing; accelerated imaging; parallel imaging; whole-heart coronary MRI; sub-millimeter; high resolution imaging

---

## Introduction

Coronary artery disease (CAD) remains the leading cause of death in the United States, accounting for one of every six deaths, despite significant efforts in prevention and treatment (1). The current clinical gold standard for the diagnosis of CAD is catheter-based invasive x-ray angiography. A recent study of nearly 400,000 patients referred for x-ray coronary angiography showed that only less than 40% had obstructive CAD, a relatively low yield for an invasive test (2). Therefore, alternative non-invasive imaging modalities, such as multi-detector computed tomography (MDCT) and coronary MRI has the potential to be a gate-keeper to invasive coronary x-ray angiography. Coronary MDCT has the advantage of rapid imaging and superior isotropic spatial resolution on the order of  $0.6 \times 0.6 \times 0.6 \text{ mm}^3$ . Coronary MRI, on the other hand, is advantageous to MDCT in several respects, since it does not require ionizing radiation or iodinated contrast, thereby facilitating follow-up scanning, and it has smaller artifacts related to epicardial calcium.

Though there have been advances over the last decade, coronary MRI remains challenging due to long scan times, limited spatial resolution, low signal-to-noise-ratio (SNR) and low blood-myocardium contrast-to-noise-ratio (CNR). Several approaches have been utilized to address these limitations, including the application of  $T_2$  magnetization preparation technique (3,4), more efficient k-space sampling (5,6), administration of vasodilators (7), imaging at higher magnetic field strengths (8–10), and the use of exogenous contrast agents (11–21). Recently, it was shown that a sub-millimeter acquisition with a spatial resolution of  $0.35 \times 0.35 \times 1.5 \text{ mm}^3$  may allow for improved detection of stenosis for targeted coronary MRI (22). However, such high-resolution targeted acquisitions require a 9 minute scan time per vessel assuming 100% navigator gating efficiency. A whole-heart coronary MRI scan with 1 mm isotropic spatial resolution results in a 16 min acquisition time assuming a heart rate of 70 bpm and 100% navigator gating efficiency. Thus to achieve whole-heart coverage and sub-mm isotropic spatial resolution, accelerated imaging is required.

Non-Cartesian trajectories (23), or parallel imaging techniques such as generalized autocalibrating partially parallel acquisition (GRAPPA) (18,20) or sensitivity encoding (SENSE) (19,24) have been utilized in previous studies to reduce the scan time of coronary MRI, with resultant acceleration rates of up to 2-fold while using 5 to 16 element cardiac-coil arrays, and up-to 4-fold acceleration rate using 32-channel coils (25,26). Currently, parallel imaging is considered the state-of-the-art accelerated imaging technique for whole-heart coronary MRI, and is commonly utilized for clinical imaging.

Compressed sensing (CS) is an alternative image reconstruction method for accelerated acquisitions with incoherently undersampled k-space data that exploits the sparsity of the image in a transform domain (27,28). CS also requires an incoherent undersampling pattern, which can be achieved by random undersampling of k-space data in the  $k_y$ - $k_z$  plane for

three-dimensional (3D) Cartesian acquisitions. In pediatric MRI, a combination of CS and parallel imaging outperforms parallel imaging alone, when a randomly undersampled k-space is used for both reconstruction techniques (29). In high-resolution CMR, an improved CS-based reconstruction strategy for randomly undersampled data, called Low-dimensional-structure Self-learning and Thresholding (LOST) provides reconstructions with reduced blurring compared to conventional CS techniques (30), and was successfully utilized in contrast-enhanced whole-heart coronary MRI (21), as well as accelerated isotropic resolution late gadolinium enhancement imaging (31). While these studies have demonstrated that a prospectively randomly undersampled k-space with CS reconstruction can be used clinically, a head-to-head comparison of such CS techniques utilizing prospective random k-space undersampling versus parallel imaging with prospective uniform undersampling has not been performed.

In this study, we sought to enable highly-accelerated acquisition of sub-mm resolution (0.9 mm isotropic) whole-heart coronary MRI, using a prospective random undersampling of k-space and an image reconstruction technique combining parallel imaging and LOST, thereby reducing the scan time to ~6 minutes. We further sought to compare this CS technique to parallel imaging with uniform undersampling, the current state-of-the-art in accelerated coronary MRI, where both techniques were used at acceleration rates beyond what is used clinically.

## Methods

All imaging sequences were implemented on a 1.5-T Philips Achieva (Philips Healthcare, Best, The Netherlands) system with a 32-channel cardiac phased-array receiver coil. For this HIPAA-compliant study, the imaging protocol was approved by our institutional review board. Written informed consent was obtained from all participants.

### Accelerated Sub-Millimeter Coronary MRI

Seven healthy adult subjects ( $30.3 \pm 12.1$  years, 3 men) underwent coronary MRI. Scout images were acquired with a SSFP sequence with  $3.1 \times 3.1$  mm<sup>2</sup> in-plane resolution and 10 mm slice thickness. This was followed by a breath-held high-temporal-resolution cine steady state free precession (SSFP) image in the 2-chamber view (TR/TE = 3.7/1.8 ms; temporal resolution = 48 msec; spatial resolution =  $1.7 \times 1.7$  mm<sup>2</sup>) to visually identify the quiescent period of the right coronary artery (RCA), which was subsequently used as the electrocardiogram (ECG) trigger delay for whole-heart coronary MRI. A subject-specific acquisition window was used, ranging between 80 and 125 ms.

Whole-heart coronary MRI was acquired using a free-breathing ECG-triggered navigator-gated SSFP sequence with isotropic sub-mm spatial resolution ( $0.9 \times 0.9 \times 0.9$  mm<sup>3</sup>). Images were acquired in the coronal plane with a field-of-view =  $290 \times 290 \times 100$  mm<sup>3</sup>. A truncated RF excitation pulse (flip angle = 90°) was used for a reduced repetition time and echo time of 4.0 ms and 2.0 ms respectively. A T<sub>2</sub> magnetization preparation pulse (TE = 50 ms) and a spectrally selective fat-saturation sequence were used to improve contrast between coronary arteries and surrounding myocardium and fat. A navigator placed on the dome of the right hemidiaphragm was used for respiratory motion compensation, utilizing prospective real-

time correction with a 5 mm end-expiration gating window and 0.6 superior-inferior tracking ratio (32,33). Saturation bands were used to reduce fold-over artifacts in the phase encode direction.

Two separate accelerated acquisitions were performed for this study. For the SENSE-based approach, the data acquisition was prospectively accelerated using uniform undersampling (3-fold in  $k_y$  and 2-fold  $k_z$ ), using the commercially available pulse sequence. For the LOST-based approach, the data acquisition was prospectively accelerated by a rate of 6 in  $k_y$ - $k_z$  using a pseudo-randomly generated undersampling pattern. Central k-space corresponding to 3% of the k-space was fully-sampled, and the outer k-space was randomly undersampled. A modified radial  $k_y$ - $k_z$  phase reordering scheme was used to mitigate flow artifacts and Eddy currents by reducing gradient switching (21). A brief description of this technique is available in Appendix A. The order of the two accelerated acquisitions was randomized.

### Image Reconstruction

The acquired raw data for the randomly undersampled CS acquisitions were exported from the scanner and images were reconstructed offline using an iterative  $B_1$ -weighted LOST algorithm. In a previous study, LOST algorithm was shown to improve on existing CS methods in terms of image sharpness for coronary MRI (30). Briefly, in this approach, an image estimate is used to adaptively identify 2D image blocks of similar signal content, which are grouped into similarity clusters. For each voxel of the image, the  $N_b \times N_b$  reference block whose top left corner is at that voxel is compared using the normalized  $l_2$  distance to another block. These blocks are declared to be similar if this distance is less than a threshold,  $\lambda_{\text{match}}$ , and the compared block is added to the similarity cluster of that voxel. Then a 3D fast Fourier transform (FFT) is applied to each similarity cluster to adaptively sparsify the data (30). Thresholding of the data is performed via the shrinkage of the 3D FFT coefficients of the similarity clusters.

In the iterative  $B_1$ -weighted reconstruction approach, the coil sensitivity information is used for data consistency during the reconstruction (34,35). Coil sensitivity maps were generated from the fully-sampled central k-space using Hanning filtering in the  $k_y$ - $k_z$  direction. At every iteration of the  $B_1$ -weighted LOST algorithm: (1) The current combined-coil image estimate was thresholded using LOST as described, (2) The combined image was mapped to individual coils via voxel-wise multiplication with the sensitivity map of that coil, (3) Data consistency with the measured data was enforced by Fourier transforming the coil images, replacing the acquired k-space locations with the acquired lines, and inverse Fourier transforming to get data-consistent images, (4) The data-consistent coil images were combined using the coil sensitivity maps, where the voxel-wise product of the coil images and conjugate of the coil sensitivity maps were summed across the coil dimension, to generate the next image estimate. The algorithm is summarized in Figure 1.

LOST reconstruction was implemented in Matlab (v7.6, MathWorks, Natick, MA), with the adaptive learning and nonlinear shrinkage portions implemented in C++. The details of the implementation, as well as the reconstruction parameters are described in Appendix B. The same reconstruction parameters were used in all cases, allowing for fully automated

reconstructions. Comparison images for SENSE were generated using the commercially available scanner software. The reconstruction resolution for the final LOST images and the SENSE images was  $0.45 \times 0.45 \times 0.45 \text{ mm}^3$ .

### Image and Statistical Analysis

Subjective image scores were used to evaluate the LOST and SENSE reconstructions for all datasets. A qualitative assessment of coronary artery image quality was performed by an experienced independent blinded reader with coronary MRI experience, using a four-point scale system (36): 1, poor or uninterpretable (coronary artery visible, with markedly blurred borders and edges); 2, fair (coronary artery visible, with moderately blurred borders and edges); 3, good (coronary artery visible, with mildly blurred borders and edges); 4, excellent (coronary artery visible, with sharply defined borders and edges). Separate scores were given for the proximal, mid, and distal segments of the RCA, the left anterior descending artery (LAD) and the left circumflex artery (LCX); and for the left main artery (LM). Additionally, an overall image score for the visualization of coronaries was given for each subject. Due to the difficulty of SNR quantification for CS techniques, which inherently threshold and shrink the noise, a perceived SNR score was given (29) on a four-point scale (1, lowest; 4, highest). The signed rank test was used for imaging scores to test for the null hypothesis that the central tendency of the difference was zero for the two reconstructions. All statistical analyses were performed using SAS (v9.3, SAS Institute, Cary, NC). A *P* value of  $<0.05$  was considered to be significant.

A SoapBubble tool (37) was used to quantitatively evaluate vessel sharpness for RCA, LAD and LCX, using the proximal and mid segments. Vessel sharpness scores were calculated for both sides of the vessel using a Deriche algorithm (38). Final normalized sharpness was defined as the average score of both sides divided by the center of vessel intensity.

### Results

Sub-mm whole-heart coronary MRI scanning was successfully completed in all subjects with both methods and without complications. The nominal scan time for these acquisitions was 3:30 minutes at 70 heart-beats per min, assuming 100% navigator gating efficiency. The average scan time was  $6:06 \pm 1:24$  minutes (range 3:56 and 7:40 minutes) for LOST, and  $6:09 \pm 1:13$  (range 4:32 to 7:39 minutes) for SENSE (*P* = NS). The corresponding average NAV gating efficiencies were  $59.7 \pm 13.1\%$  (range: 49.5% and 86.5%) and  $58.0 \pm 8.5\%$  (range: 50.5% and 75.1%) respectively (*P* = NS), with an overall average NAV gating efficiency of  $58.8 \pm 10.6\%$ . The difference between the nominal scan time and the actual average scan time are due to differences in breathing patterns and heart rates of the subjects. The reconstruction time for the  $B_1$ -weighted LOST algorithm was approximately 90 minutes.

Figure 2 depicts an example coronal slice and reformatted coronal image from one of the acquisitions, showing a cross-section of the LAD, and long axis of the RCA and LCX of the subject respectively, reconstructed with LOST and SENSE. The LAD is clearly visualized in the coronal cross-section with the proposed  $B_1$ -weighted LOST approach, whereas noise amplification in the SENSE image is apparent, and the visualization of the LAD is hindered.

The reformatted images also show the different levels of noise amplification, although the effect is less visible due to the reformatting. Figure 3 shows axial reformats from a different subject. Both noise amplification and folding artifacts in the anterior-posterior direction are visible in the SENSE images depicting the proximal RCA and LAD. These artifacts are not produced with the LOST approach, where both branches are visualized clearly. Example coronal cross-section and reformatted coronal slices in another subject are depicted in Figure 4, which demonstrates high levels of noise amplification in the SENSE reconstruction. In this case, the LM coronary artery is not visible due to noise, and the proximal LCX and distal RCA cannot be tracked for reformatting in the SENSE images. All the coronary arteries, including the distal sections are shown with improved definition using the LOST approach.

Table 1 summarizes the qualitative coronary MRI assessment for the LOST and the SENSE reconstructions from the randomly undersampled and uniformly undersampled acquisitions respectively. The scores for all coronary artery branches were higher for LOST, although the difference was statistically significant for only the mid LCX branch. The overall image score for LOST was significantly higher than that of SENSE ( $3.1 \pm 0.7$  vs.  $2.1 \pm 0.9$ ,  $P = 0.03$ ). The perceived SNR score was also significantly higher for LOST ( $3.4 \pm 0.8$  vs.  $2.4 \pm 1.1$ ,  $P = 0.03$ ). Vessel sharpness measurements were completed on all subjects, except two, where the LAD and LCX were not visible in the SENSE images. These coronary branches of the two subjects were excluded from further analysis. The vessel sharpness values for LOST and SENSE were as follows:  $0.60 \pm 0.06$  vs.  $0.57 \pm 0.06$  ( $P = 0.02$ ) for the RCA ( $N = 7$ );  $0.61 \pm 0.05$  vs.  $0.59 \pm 0.05$  ( $P = 0.18$ ) for the LAD ( $N = 5$ );  $0.61 \pm 0.06$  vs.  $0.59 \pm 0.03$  ( $P = 0.17$ ) for the LCX ( $N = 5$ ).

## Discussion

In this study, we have demonstrated the efficacy of an accelerated isotropic sub-millimeter whole-heart coronary MRI method utilizing a prospective random undersampling scheme and the  $B_1$ -weighted LOST reconstruction technique. These reconstruction and acquisition techniques allow for high-quality visualization of all coronary branches, with 6-fold accelerated acquisitions. Among a healthy group of subjects, the technique was found to be superior to parallel imaging with uniform undersampling in terms of overall quality and perceived SNR at the same acceleration rate.

Compressed sensing techniques have been utilized in numerous MRI applications, however, its utility in clinical settings has been limited, since its advantages over existing methods have not been clearly demonstrated. Much work on CS has been based on reconstruction techniques with retrospective undersampling of fully sampled data, which fails to capture realistic scenarios. Prospective Cartesian random undersampling has been utilized in previous studies (21,29,39–43). Furthermore, comparison to parallel imaging have also been provided, where the parallel imaging reconstruction has been used with the same random undersampling pattern (29), although this approach results in performance deterioration for parallel imaging techniques (44). Hence, use of uniform undersampling for parallel imaging techniques is important for a fair comparison between these techniques. In an earlier study, comparison examples between SENSE with a uniformly undersampled acquisition and CS



with prospectively random undersampled acquisition were provided (30), however a thorough comparison between the two methods were not performed. To the best of our knowledge, this work provides the first detailed head-to-head comparison between CS with prospective random undersampling and parallel imaging with prospective uniform undersampling in high-resolution cardiac MR, and highlights the advantages of CS methods for highly-accelerated low SNR applications.

The qualitative image scores indicate that the proposed method performs particularly well in proximal and mid segments, where the most clinically significant lesions occur (36). Distal segments were scored lower for both accelerated techniques, presumably because of the low SNR and CNR in these segments due to the high spatial resolution. Contrast agents have been shown to improve SNR and CNR in the distal branches of the coronaries (19). In this study, we used a non-contrast enhanced coronary MRI technique to allow for two acquisitions with different undersampling patterns, without being affected by contrast washout and changes in inversion time. Use of contrast agents may improve the visibility of the distal branches, however the utility of a contrast-enhanced coronary MRI sequence at this spatial resolution was not studied.

While vessel sharpness measurements were provided in this study, these may not be a good indicator of image quality in this setting for a number of reasons. First, the SENSE reconstruction is processed by the commercial reconstruction software, which applies additional filters that are not available on the raw data that is used to reconstruct the compressed sensing images. Second, vessel sharpness does not necessarily provide information about noise, the main source of difference of image quality in this study, as exemplified by the discrepancy between the perceived SNR and the vessel sharpness measurements. However, the measurements were included for completeness, but its utility in comparing reconstructions from different acquisitions with different processing may be limited.

Our study has several limitations. Only a small number of healthy adult subjects were studied. Further studies are needed to study the clinical evaluation and potential benefits of the improved resolution of the proposed approach in a larger cohort with well-defined CAD. We also note that the average NAV gating efficiency of most patient populations are around 30–50%, which is lower than that of the healthy cohort in this study, and this will lead to longer scan times. The reconstruction time of the proposed algorithm is too long for routine clinical use. As with other CS studies, we have not provided absolute SNR/CNR measurements comparing the two reconstructions, since a reliable characterization of the noise signal is not available for the nonlinear CS reconstruction techniques (21,29).

## Conclusion

We have demonstrated that a  $B_1$ -weighted LOST technique provides 6-fold acceleration of sub-mm whole heart coronary MRI, resulting in scan times of ~6 minutes. For such low SNR applications, the proposed CS approach with random undersampling may be more appropriate than parallel imaging with uniform undersampling.

## Acknowledgments

Supported by NIH R01EB008743-01A2, NIH K99HL111410-01.

## References

1. Lloyd-Jones D, Adams RJ, Brown TM, Carnethon M, Dai S, De Simone G, Ferguson TB, Ford E, Furie K, Gillespie C, Go A, Greenlund K, Haase N, Hailpern S, Ho PM, Howard V, Kissela B, Kittner S, Lackland D, Lisabeth L, Marelli A, McDermott MM, Meigs J, Mozaffarian D, Mussolino M, Nichol G, Roger VL, Rosamond W, Sacco R, Sorlie P, Thom T, Wasserthiel-Smoller S, Wong ND, Wylie-Rosett J. Heart disease and stroke statistics--2010 update: a report from the American Heart Association. *Circulation*. 2010; 121(7):e46–e215. [PubMed: 20019324]
2. Patel MR, Peterson ED, Dai D, Brennan JM, Redberg RF, Anderson HV, Brindis RG, Douglas PS. Low diagnostic yield of elective coronary angiography. *N Engl J Med*. 2010; 362(10):886–895. [PubMed: 20220183]
3. Brittain JH, Hu BS, Wright GA, Meyer CH, Macovski A, Nishimura DG. Coronary angiography with magnetization-prepared T2 contrast. *Magn Reson Med*. 1995; 33(5):689–696. [PubMed: 7596274]
4. Botnar RM, Stuber M, Danias PG, Kissinger KV, Manning WJ. Improved coronary artery definition with T2-weighted, free-breathing, three-dimensional coronary MRA. *Circulation*. 1999; 99(24):3139–3148. [PubMed: 10377077]
5. Meyer CH, Hu BS, Nishimura DG, Macovski A. Fast spiral coronary artery imaging. *Magn Reson Med*. 1992; 28(2):202–213. [PubMed: 1461123]
6. Bhat H, Ge L, NIELLES-Vallespin S, Zuehlsdorff S, Li D. 3D radial sampling and 3D affine transform-based respiratory motion correction technique for free-breathing whole-heart coronary MRA with 100% imaging efficiency. *Magn Reson Med*. 2011; 65(5):1269–1277. [PubMed: 21500255]
7. Hu P, Chuang ML, Ngo LH, Stoeck CT, Peters DC, Kissinger KV, Goddu B, Goepfert LA, Manning WJ, Nezafat R. Coronary MR imaging: effect of timing and dose of isosorbide dinitrate administration. *Radiology*. 2010; 254(2):401–409. [PubMed: 20093512]
8. Nezafat R, Ouwerkerk R, Derbyshire AJ, Stuber M, McVeigh ER. Spectrally selective B1-insensitive T2 magnetization preparation sequence. *Magn Reson Med*. 2009; 61(6):1326–1335. [PubMed: 19319903]
9. van Elderen SG, Versluis MJ, Westenberg JJ, Agarwal H, Smith NB, Stuber M, de Roos A, Webb AG. Right coronary MR angiography at 7 T: a direct quantitative and qualitative comparison with 3 T in young healthy volunteers. *Radiology*. 2010; 257(1):254–259. [PubMed: 20851943]
10. Gharib AM, Abd-Elmoniem KZ, Herzka DA, Ho VB, Locklin J, Tzatha E, Stuber M, Pettigrew RI. Optimization of coronary whole-heart MRA free-breathing technique at 3 Tesla. *Magn Reson Imaging*. 2011; 29(8):1125–1130. [PubMed: 21871751]
11. Knuesel PR, Nanz D, Wolfensberger U, Saranathan M, Lehning A, Luescher TF, Marincek B, von Schulthess GK, Schwitler J. Multislice breath-hold spiral magnetic resonance coronary angiography in patients with coronary artery disease: effect of intravascular contrast medium. *J Magn Reson Imaging*. 2002; 16(6):660–667. [PubMed: 12451579]
12. Paetsch I, Jahnke C, Barkhausen J, Spuentrup E, Cavagna F, Schnackenburg B, Huber M, Stuber M, Fleck E, Nagel E. Detection of coronary stenoses with contrast enhanced, three-dimensional free breathing coronary MR angiography using the gadolinium-based intravascular contrast agent gadocoletic acid (B-22956). *J Cardiovasc Magn Reson*. 2006; 8(3):509–516. [PubMed: 16755840]
13. Prompona M, Cyran C, Nikolaou K, Bauner K, Reiser M, Huber A. Contrast-enhanced whole-heart MR coronary angiography at 3.0 T using the intravascular contrast agent gadofosveset. *Invest Radiol*. 2009; 44(7):369–374. [PubMed: 19554666]
14. Goldfarb JW, Edelman RR. Coronary arteries: breath-hold, gadolinium-enhanced, three-dimensional MR angiography. *Radiology*. 1998; 206(3):830–834. [PubMed: 9494509]



15. Zheng J, Bae KT, Woodard PK, Haacke EM, Li D. Efficacy of slow infusion of gadolinium contrast agent in three-dimensional MR coronary artery imaging. *J Magn Reson Imaging*. 1999; 10(5):800–805. [PubMed: 10548791]
16. Li D, Carr JC, Shea SM, Zheng J, Deshpande VS, Wielopolski PA, Finn JP. Coronary arteries: magnetization-prepared contrast-enhanced three-dimensional volume-targeted breath-hold MR angiography. *Radiology*. 2001; 219(1):270–277. [PubMed: 11274569]
17. Weber OM, Martin AJ, Higgins CB. Whole-heart steady-state free precession coronary artery magnetic resonance angiography. *Magn Reson Med*. 2003; 50(6):1223–1228. [PubMed: 14648570]
18. Bi X, Carr JC, Li D. Whole-heart coronary magnetic resonance angiography at 3 Tesla in 5 minutes with slow infusion of Gd-BOPTA, a high-relaxivity clinical contrast agent. *Magn Reson Med*. 2007; 58(1):1–7. [PubMed: 17659628]
19. Hu P, Chan J, Ngo LH, Smink J, Goddu B, Kissinger KV, Goepfert L, Hauser TH, Rofsky NM, Manning WJ, Nezafat R. Contrast-enhanced whole-heart coronary MRI with bolus infusion of gadobenate dimeglumine at 1.5 T. *Magn Reson Med*. 2011; 65(2):392–398. [PubMed: 21264933]
20. Yang Q, Li K, Liu X, Bi X, Liu Z, An J, Zhang A, Jeremic R, Li D. Contrast-enhanced whole-heart coronary magnetic resonance angiography at 3.0-T: a comparative study with X-ray angiography in a single center. *J Am Coll Cardiol*. 2009; 54(1):69–76. [PubMed: 19555843]
21. Akçakaya M, Basha TA, Chan RH, Rayatzadeh H, Kissinger KV, Goddu B, Goepfert LA, Manning WJ, Nezafat R. Accelerated contrast-enhanced whole-heart coronary MRI using low-dimensional-structure self-learning and thresholding. *Magn Reson Med*. 2012; 67(5):1434–1443. [PubMed: 22392654]
22. Gharib AM, Abd-Elmoniem KZ, Ho VB, Fodi E, Herzka DA, Ohayon J, Stuber M, Pettigrew RI. The feasibility of 350 µm spatial resolution coronary magnetic resonance angiography at 3 T in humans. *Invest Radiol*. 2012; 47(6):339–345. [PubMed: 22551651]
23. Bhat H, Yang Q, Zuehlsdorff S, Li K, Li D. Contrast-enhanced whole-heart coronary magnetic resonance angiography at 3 T with radial EPI. *Magn Reson Med*. 2011; 66(1):82–91. [PubMed: 21305601]
24. Tang L, Merkle N, Schar M, Korosoglou G, Solaiyappan M, Hombach V, Stuber M. Volume-targeted and whole-heart coronary magnetic resonance angiography using an intravascular contrast agent. *J Magn Reson Imaging*. 2009; 30(5):1191–1196. [PubMed: 19856454]
25. Nagata M, Kato S, Kitagawa K, Ishida N, Nakajima H, Nakamori S, Ishida M, Miyahara M, Ito M, Sakuma H. Diagnostic accuracy of 1.5-T unenhanced whole-heart coronary MR angiography performed with 32-channel cardiac coils: initial single-center experience. *Radiology*. 2011; 259(2):384–392. [PubMed: 21406635]
26. Niendorf T, Hardy CJ, Giaquinto RO, Gross P, Cline HE, Zhu Y, Kenwood G, Cohen S, Grant AK, Joshi S, Rofsky NM, Sodickson DK. Toward single breath-hold whole-heart coverage coronary MRA using highly accelerated parallel imaging with a 32-channel MR system. *Magn Reson Med*. 2006; 56(1):167–176. [PubMed: 16755538]
27. Block KT, Uecker M, Frahm J. Undersampled radial MRI with multiple coils. Iterative image reconstruction using a total variation constraint. *Magn Reson Med*. 2007; 57(6):1086–1098. [PubMed: 17534903]
28. Lustig M, Donoho DL, Pauly JM. Sparse MRI: The application of compressed sensing for rapid MR imaging. *Magn Reson Med*. 2007; 58(6):1182–1195. [PubMed: 17969013]
29. Vasanawala SS, Alley MT, Hargreaves BA, Barth RA, Pauly JM, Lustig M. Improved pediatric MR imaging with compressed sensing. *Radiology*. 2010; 256(2):607–616. [PubMed: 20529991]
30. Akçakaya M, Basha TA, Goddu B, Goepfert LA, Kissinger KV, Tarokh V, Manning WJ, Nezafat R. Low-dimensional-structure self-learning and thresholding: Regularization beyond compressed sensing for MRI Reconstruction. *Magn Reson Med*. 2011; 66(3):756–767. [PubMed: 21465542]
31. Akçakaya M, Rayatzadeh H, Basha TA, Hong SN, Chan RH, Kissinger KV, Hauser TH, Josephson ME, Manning WJ, Nezafat R. Accelerated late gadolinium enhancement cardiac MR imaging with isotropic spatial resolution using compressed sensing: initial experience. *Radiology*. 2012; 264(3):691–699. [PubMed: 22820734]

32. Wang Y, Riederer SJ, Ehman RL. Respiratory motion of the heart: kinematics and the implications for the spatial resolution in coronary imaging. *Magn Reson Med*. 1995; 33(5):713–719. [PubMed: 7596276]
33. Danias PG, Stuber M, Botnar RM, Kissinger KV, Edelman RR, Manning WJ. Relationship between motion of coronary arteries and diaphragm during free breathing: lessons from real-time MR imaging. *AJR*. 1999; 172(4):1061–1065. [PubMed: 10587147]
34. Otazo R, Kim D, Axel L, Sodickson DK. Combination of compressed sensing and parallel imaging for highly accelerated first-pass cardiac perfusion MRI. *Magn Reson Med*. 2010; 64(3):767–776. [PubMed: 20535813]
35. Akçakaya M, Nam S, Hu P, Moghari MH, Ngo LH, Tarokh V, Manning WJ, Nezafat R. Compressed sensing with wavelet domain dependencies for coronary MRI: a retrospective study. *IEEE Trans Med Imaging*. 2011; 30(5):1090–1099. [PubMed: 21536523]
36. Kim WY, Danias PG, Stuber M, Flamm SD, Plein S, Nagel E, Langerak SE, Weber OM, Pedersen EM, Schmidt M, Botnar RM, Manning WJ. Coronary magnetic resonance angiography for the detection of coronary stenoses. *N Engl J Med*. 2001; 345(26):1863–1869. [PubMed: 11756576]
37. Etienne A, Botnar RM, Van Muiswinkel AM, Boesiger P, Manning WJ, Stuber M. “Soap-Bubble” visualization and quantitative analysis of 3D coronary magnetic resonance angiograms. *Magn Reson Med*. 2002; 48(4):658–666. [PubMed: 12353283]
38. Deriche R. Fast algorithms for low-level vision. *IEEE Transactions on Pattern Analysis and Machine Intelligence*. 1990; 12(1):78–87.
39. Otazo, R.; Xu, J.; Axel, L.; Sodickson, D. Combination of compressed sensing and parallel imaging for highly-accelerated 3D first-pass cardiac perfusion MRI. 2010 May; Stockholm. Proceedings of the 18th Scientific Meeting of ISMRM; p. 344
40. Kim YC, Narayanan SS, Nayak KS. Accelerated three-dimensional upper airway MRI using compressed sensing. *Magn Reson Med*. 2009; 61(6):1434–1440. [PubMed: 19353675]
41. Feng L, Srichai MB, Lim RP, Harrison A, King W, Adluru G, Dibella EV, Sodickson DK, Otazo R, Kim D. Highly accelerated real-time cardiac cine MRI using k-t SPARSE-SENSE. *Magn Reson Med*. 2012 [Epub ahead of print]. 10.1002/mrm.24440
42. Kim D, Dyvorne HA, Otazo R, Feng L, Sodickson DK, Lee VS. Accelerated phase-contrast cine MRI using k-t SPARSE-SENSE. *Magn Reson Med*. 2012; 67(4):1054–1064. [PubMed: 22083998]
43. Kwak Y, Nam S, Akçakaya M, Basha TA, Goddu B, Manning WJ, Tarokh V, Nezafat R. Accelerated aortic flow assessment with compressed sensing with and without use of the sparsity of the complex difference image. *Magn Reson Med*. 2012 [Epub ahead of print]. 10.1002/mrm.24514
44. Pruessmann KP, Weiger M, Bornert P, Boesiger P. Advances in sensitivity encoding with arbitrary k-space trajectories. *Magn Reson Med*. 2001; 46(4):638–651. [PubMed: 11590639]

## Appendix A

### Profile Ordering for Random Undersampling of k-space

We summarize the profile ordering for random k-space undersampling described in (21) for completeness. First a pseudo-random  $k_y$ - $k_z$  undersampling mask is generated, which includes the center of k-space of pre-defined size. In segmented acquisition, the k-space lines from this mask are divided into different shots, where a *shot* is a group of lines that are acquired in one heartbeat. Each shot of the segmented coronary MRI acquisition, 20–25  $k_y$ - $k_z$  lines are sampled depending on the length of the subject-specific acquisition window. The division of the lines into different shots, and the acquisition order of the lines within each shot follows a specific profile ordering scheme: 1) Each k-space line is assigned magnitude and phase values based on its location in  $k_y$ - $k_z$  plane (i.e. magnitude =  $\sqrt{k_y^2 + k_z^2}$  and phase =  $\text{atan}(k_z/k_y)$ ), 2) Lines are assigned to different shots based on their phase values,

such that a line with lower phase value is assigned to an earlier shot during the acquisition, 3) Within each shot, lines are sorted based on their magnitude values, such that a line with lower magnitude value is acquired first in the shot. As described in (21), this results in our proposed modified radial acquisition scheme that helps reducing the k-space jumps during the acquisition.

## Appendix B

### Implementation Details of $B_1$ -weighted LOST

The  $B_1$ -weighted LOST algorithm was implemented in two stages. For the first stage, the coil sensitivity information was used with total variation denoising to generate an initial image estimate. This was used for identification of similarity clusters, with parameters  $N_b = 4$ ,  $\lambda_{\text{match}} = 0.05$ . For each reference block, comparison with other blocks was limited to a neighborhood of radius 6 in  $x$ - $y$  and of radius 1 in  $z$  direction. The maximum number of blocks in a similarity cluster was limited to 8. During the second stage, data consistency using coil sensitivity information and LOST shrinkage were performed at every iteration, for a total of 25 iterations. For shrinkage, LOST alternated between hard thresholding and Wiener filtering, with thresholding parameters  $\tau_{\text{ht}}$  and  $\tau_{\text{wic}}$  respectively set to 0.015 and 0.02 times the largest coefficient of the estimate from the first stage.

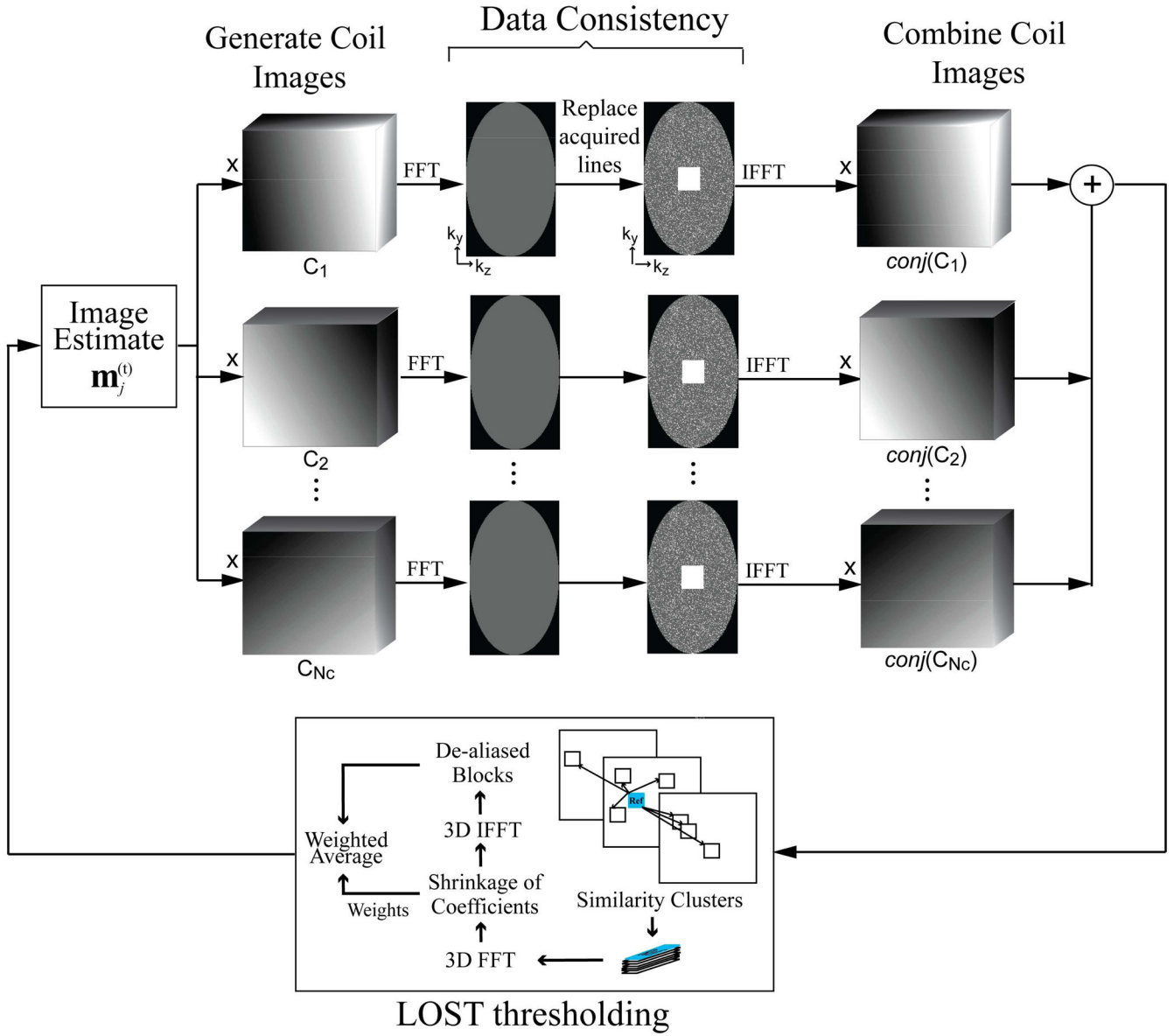


**Figure 1.** Schematic for a single iteration of the B<sub>1</sub>-weighted LOST algorithm used in this study. At every iteration, the current image estimate is mapped to individual coil images by voxel-wise multiplication with sensitivity maps. Data consistency is enforced by replacing the acquired k-space lines. A combined image is generated by summing the voxel-wise product of data-consistent coil images and conjugate of coil sensitivity maps across the coil dimension. This image is then thresholded using LOST. The implementation details of LOST thresholding are given in the Appendix.

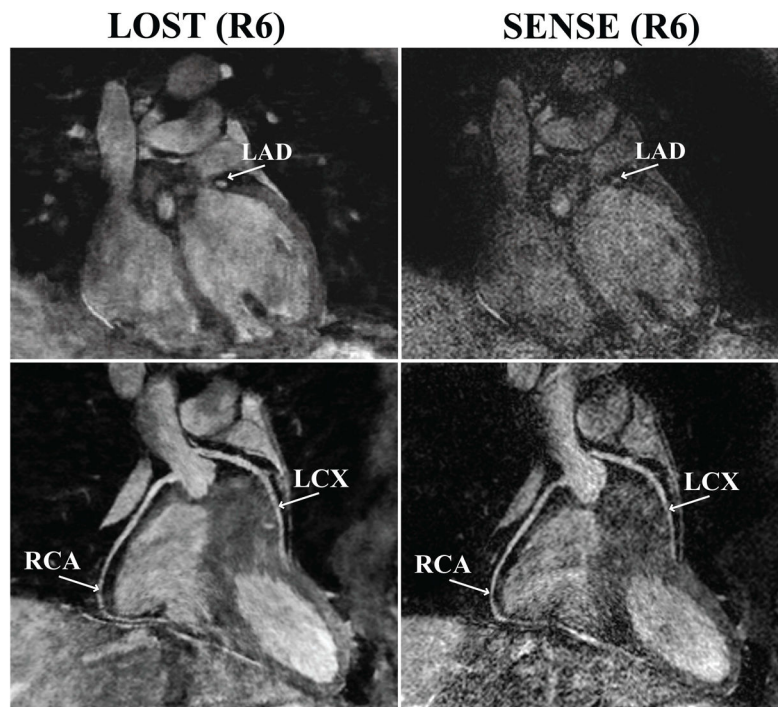


**Figure 2.**

An example coronal slice (top) and reformatted coronal image (bottom) of a subject using  $B_1$ -weighted LOST with 6-fold random undersampling (left) and SENSE with 6-fold uniform undersampling. A cross-section of the LAD is visualized clearly with the proposed technique, whereas noise amplification is apparent in the SENSE-reconstructed image (RCA: right coronary artery, LAD: left anterior descending, LCX: left circumflex).

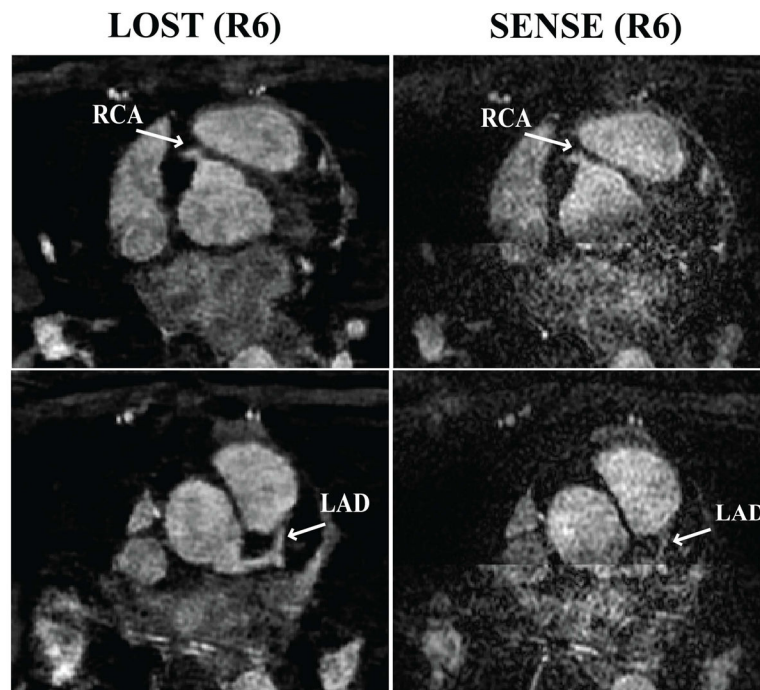


**Figure 3.** Example axial reformats using  $B_1$ -weighted LOST with 6-fold random undersampling (left) and SENSE with 6-fold uniform undersampling. Noise amplification and SENSE folding artifacts in the z-direction (anterior-posterior) are apparent in both of the slices depicting the proximal RCA and the proximal LAD. Similar artifacts are not visible in the proposed LOST technique.



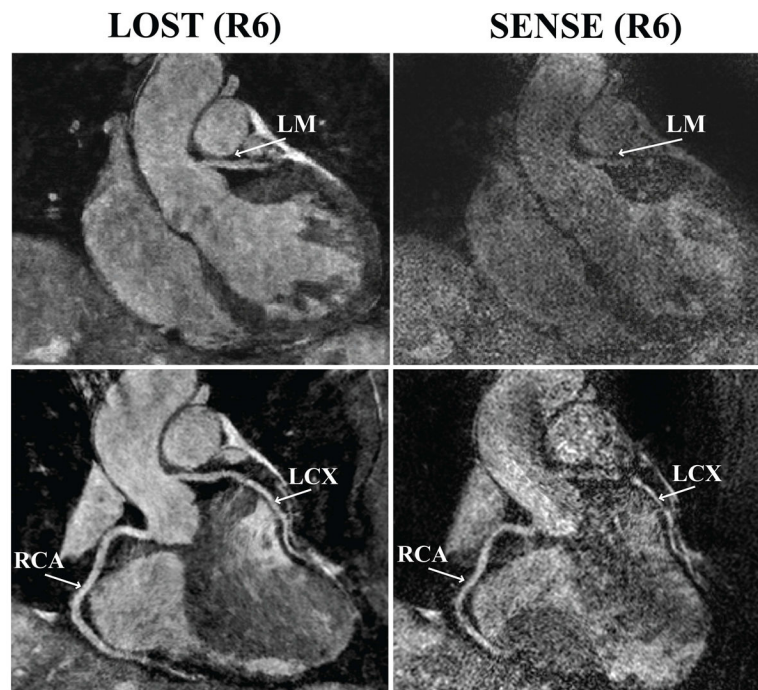


**Figure 4.**

An example coronal slice (top) containing a cross-section of the left main (LM) shows that SENSE images with 6-fold uniform undersampling (right) suffers from noise amplification, whereas the LM is clearly visualized using  $B_1$ -weighted LOST with 6-fold random undersampling (left). In the reformatted coronal images (bottom), the proximal LCX cannot be tracked due to the high noise level in the SENSE reconstruction, but RCA and LCX branches are avisualized with the LOST technique.

**Table 1**

Comparison of average subjective imaging scores (1 = poor, 2 = fair, 3 = good, 4 = excellent) between SENSE reconstruction with 6-fold uniform undersampling and B<sub>1</sub>-weighted LOST reconstruction with 6-fold random undersampling. LOST was evaluated higher for all branches. The differences were statistically significant for overall score and perceived SNR score, as well as the mid-LCX. A *P*-value less than 0.05 was considered significant.

|                 | PROXIMAL  |           |           |           | MID       |           |           |           | DISTAL    |           |           |           | OVERALL | PERCEIVED SNR |
|-----------------|-----------|-----------|-----------|-----------|-----------|-----------|-----------|-----------|-----------|-----------|-----------|-----------|---------|---------------|
|                 | RCA       | LAD       | LCX       | RCA       | LAD       | LCX       | RCA       | LAD       | LCX       | RCA       | LAD       | LCX       |         |               |
| SENSE           | 3.1 ± 0.9 | 2.4 ± 1.3 | 2.4 ± 1.3 | 2.3 ± 1.1 | 2.6 ± 1.3 | 1.9 ± 0.9 | 2.3 ± 1.1 | 2.3 ± 1.0 | 1.7 ± 1.0 | 2.7 ± 1.1 | 2.1 ± 0.9 | 2.4 ± 1.1 |         |               |
| LOST            | 3.6 ± 0.5 | 3.7 ± 0.5 | 3.4 ± 0.8 | 3.0 ± 0.8 | 3.1 ± 0.7 | 2.7 ± 0.8 | 2.6 ± 1.1 | 3.0 ± 1.2 | 2.0 ± 1.3 | 3.7 ± 0.5 | 3.1 ± 0.7 | 3.4 ± 0.8 |         |               |
| <i>P</i> -value | 0.50      | 0.06      | 0.06      | 0.18      | 0.31      | 0.03      | 0.63      | 0.06      | 0.50      | 0.06      | 0.03      | 0.03      |         |               |